Journal of Thermal Analysis and Calorimetry, Vol. 66 (2001) 677–697

DATA ANALYSIS WITHOUT FOURIER TRANSFORMATION FOR SAWTOOTH-TYPE TEMPERATURE-MODULATED DSC

W. Hu and B. Wunderlich

Department of Chemistry, The University of Tennessee, Knoxville, TN 37996-1600, and Chemical and Analytical Sciences Division, Oak Ridge National Laboratory, Oak Ridge, TN 37831-6197, USA

(Received March 26, 2001)

Abstract

The response of a differential scanning calorimeter (DSC) to sawtooth-type temperature modulation has been analyzed in the time domain using a standard treatment of the DSC data without Fourier transformation into the frequency domain. This method has some of the advantages of a temperature-modulated DSC (TMDSC) and may achieve a reasonable accuracy with more transparent and less time-consuming data analysis than the current TMDSC. The limits of linearity and stationarity of the thermal response, a prerequisite for the validity of the calculation of the reversing heat capacity by Fourier transformation, can be easily recognized in standard DSC. In contrast to the common handling of TMDSC, where the non-reversing contributions are calculated as difference between the total and reversing parts, we define a new, directly measured quantity, called the imbalance in heat capacity. It represents the difference between heating and cooling due to the non-reversing thermal process. This quantity is also of value for the representation of irreversible contributions in quasi-isothermal processes, such as cold crystallization and the annealing of crystallites in the melting range.

Keywords: imbalance in heat capacities, reversing and non-reversing heat capacities, sawtooth modulation, standard DSC, TMDSC

Introduction

Temperature-modulated differential scanning calorimetry (TMDSC) [1–3] is an important development beyond conventional DSC. The common sinusoidal mode of temperature modulation as a scanning program is usually coupled with a discrete Fourier transformation for the data analysis in the frequency domain, which leads to a deconvolution of the reversing and the total heat-flow rate from which then the corresponding heat capacities are calculated and by difference the non-reversing quantity is assessed [4].

The reversing heat capacity, however, is only properly calculated under the conditions of linearity and stationarity of the thermal response [5]. Furthermore, some thermal processes lead to a heat-flow rate response such, that its first harmonic of the

1418–2874/2001/ $ 5.00

Akadémiai Kiadó, Budapest
Kluwer Academic Publishers, Dordrecht

Fourier series is not a correct representation of the reversing contribution [6, 7]. The TMDSC of samples undergoing a glass transition, for example, has been modelled using different methods [8–12]. The first harmonic represents the sample response only approximately [13–16]. It is necessary to fit the experimental data to such a model to assess the reversing and non-reversing contributions properly and to make a connection to the earlier data gained by standard dynamic differential thermal analysis (DDTA) [17]. The complete reversing thermal response to a sinusoidal modulation superimposed on a constant underlying heating rate contains not only a first, but also a second harmonic component, as well as a constant contribution, and its frequency is shifted depending on the underlying heating rate [11, 15].

For melting, crystal growth and annealing of polymers, the kinetics and irreversibility were studied over the last 70 years [18]. The processes are largely irreversible and should thus appear only in the total response to modulation and by difference in the non-reversing contribution. A TMDSC trace, thus, should be an effective tool to separate any remaining reversible processes from the irreversible ones. A model to analyze the crystallization rate at different frequencies is available [19], and the categories of reversible and irreversible effects observed in the melting range have been established [20, 21]. The analysis, however, has been proven difficult because of serious lack of linearity and stationarity, often coupled with instrument lags [6].

Heat capacity can be calculated in the standard DSC method under conditions of steady state and negligible temperature gradient within the sample. The same is true in case of sawtooth modulation where the heating and cooling segments are long enough to reach steady state before switching from heating to cooling and vice versa. The data taken during the approach to steady state must in this case be discarded, just as in standard DSC where one does not use the initial approach to standard state on start-up. If needed, it is also possible to insert occasional isotherm segments between the sawtooth modulation to monitor the baseline drift of the calorimeter. If there exists an irreversible or slow thermal process, it can be analyzed in detail in the time domain, without the previously mentioned errors in the Fourier-transform of a distorted thermal response. The precision of this simple method of modulation and its analysis is somewhat less than using detailed Fourier analyses of temperatures and heat-flow rates including the time interval before reaching steady state, but can achieve the same level as possible with the standard DSC [22]. The additional information which is generated about kinetics and irreversibility is of value and is gained without costly special instrumentation and software, and often the measurements require considerably less time.

The switching of the rate of temperature-change from one value to another in sawtooth modulation is easily realized in most of modern calorimeters, as was shown recently for the generation of high precision data for three different calorimeters [23–26]. Standard DSC analysis for this type of temperature modulation was proposed earlier [27, 28]. The recently proposed step-scan DSC [29] (alternative heating and isothermal steps) may yield similar data and was earlier proposed and applied to the standard DSC [22, 30, 31]. Quantitative comparisons of analysis by Fourier transformation to analysis by standard DSC have proved their coincidence by utilizing the

whole time interval of data with and without being in steady state by TMDSC and the much smaller time interval of being in steady state by standard DSC [24].

A final note concerns nomenclature. We will use, as customary, the term reversing when a heat effect can apparently be reversed in the time interval of the modulation period, while the term reversible is reserved for a proven thermodynamically reversible effect. The latter designation needs most often a quasi-isothermal test that proves successive cycles can be superimposed indefinitely.

In this paper, after a simple introduction of the data analysis in standard DSC and TMDSC, the advantages of sawtooth modulation evaluated by a standard DSC method are elucidated by a case analysis and measurements on poly(ethylene terephthalate). The data were compared to the recommended data in the Athas Data Bank [32].

Data analysis in standard DSC and TMDSC

Standard DSC

Fast heat capacity measurement is a characteristic of the DSC. Basic to any DSC measurement is a linear response of the heat-flow rate ($\Phi=\mathrm{d}Q/\mathrm{d}t$) to the rate of change in temperature $q=\dot{T}=\mathrm{d}T_s/\mathrm{d}t$. The value of Φ is proportional to the temperature difference $\Delta T(=T_r-T_s)$ between the reference and the sample calorimeter. For the standard DSC, if a steady state with only negligible temperature gradients within the sample holds, one can derive the following equation [33]:

$$mc_p = K\frac{\Delta T}{q} + C_s\left(\frac{\mathrm{d}\Delta T}{\mathrm{d}T_s}\right) \approx \frac{\Phi}{q} \tag{1}$$

where m is the sample mass, c_p represents the specific heat capacity of the sample, K is the Newton's law constant $q=\dot{T}$ stands for the constant rate of temperature change at steady state which is positive for heating (q_h) and negative for cooling (q_c), C_s is the heat capacity of the complete sample calorimeter consisting of sample and pan, and T_s represents the sample temperature.

With a negligible temperature gradient within the sample and no thermal resistance between sample sensor and sample pan, T_s is also the temperature of the sample sensor. The second term in the center part of the equations corrects for the larger change of C_s with temperature relative to C_r, the heat capacity of the usually empty reference calorimeter. As long as the change in difference between reference and sample temperature is negligible, $\mathrm{d}\Delta T/\mathrm{d}T_s \approx 0$, and the heat capacity is directly proportional to Φ, as shown in the far right-hand side of Eq. (1).

The key details of the measuring procedures are to maintain the validity of the discussed conditions and to carry out sufficiently accurate calibrations, to establish the actual temperature of the sample, and to evaluate K or Φ [34]. The sample temperature is usually calibrated with the onset of the melting peak of two or more melting-point standards. The values of K or Φ must be established as a function of temper-

ature by performing a calibration run, usually with sapphire as sample [35]. The asymmetry of two calorimeters must be evaluated from a baseline run of two identical empty pans and subtracted from the sample and calibration runs, as is described in standard texts [33]. The stability of the baseline during the measurement can be checked by the coincidence of the initial and final isotherm for all three runs that constitute a single measurement (sample, asymmetry and calibration). A short scanning range was suggested early [30], but is frequently disregarded and runs of several hundred kelvins have been published. When attempting to make quality heat capacity measurements, short-segment analysis is of major importance [29, 31].

Temperature-modulated DSC

In TMDSC the experiment is carried out with an underlying change of temperature, $<q>$, which is represented by the sliding average over one modulation period. The sample temperature and heat-flow rate are changing with time, as dictated by the underlying heating rate and the modulation, and are written as $T_s(t)$ and $\Phi(t)$, respectively. The measurement of c_p remains simple, as long as the condition of steady state and negligible temperature gradients within the sample can be maintained. If the sample response is linear, the sliding averages over one modulation period of T_s and Φ, written as $<T_s>$, and $<\Phi>$, yield identical curves as for the standard DSC given by Eq. (1). Next, a simple subtraction of these averages from their instantaneous values $T_s(t)$ and $\Phi(t)$, yields the pseudo-isothermal 'reversing' signals. For sinusoidal modulation of the sample temperature, the quasi-isothermal analysis has been described in detail. It yields for the heat capacity the following expression which also holds for the pseudo-isothermal analysis with an underlying rate of temperature change $<q>$ [4]:

$$(C_s - C_r) = \frac{A_\Phi}{A_q}\sqrt{1+\left(\frac{C_r\omega}{K}\right)^2} \qquad (2)$$

where A_Φ is the modulation amplitude of the heat-flow rate and A_q that of the heating rate ($=A_{T_s}\omega$).

The frequency ω is given in rad s^{-1} ($\omega=2\pi/p$, where p is the modulation period in seconds). For other than sinusoidal modulations, Eq. (2) applies independently to A_Φ and A_q for the various harmonics n with frequencies of $n\omega$. The similarity of the Eqs (1) and (2) becomes obvious if the reference calorimeter is an empty pan. Then, $C_s - C_r = mc_p$, and A_q represents the maximum amplitude of the modulation of the rate of temperature change without the effect of the underlying rate, $\dot{T}(t) - <\dot{T}>$. If calibrations and measurement are made at frequency ω with the same reference pan, the square root in Eq. (2) is constant and can be made part of a calibration constant.

The conditions of steady state and negligible temperature gradient within the calorimeters are more stringent for TMDSC than for the standard DSC, because if even a small temperature gradient is set up within the sample during the modulation, each modulation cycle has a smaller amplitude of heat-flow rate which depends on the unknown thermal conductivities and resistances. A negligible temperature gradi-

ent within the sample requires, thus, that the sample calorimeter oscillates in its entirety. It also requires a negligible thermal resistance between thermometer and pan, and the pan and sample calorimeter. The phase lag between heater and sample must in this case be entirely due to the thermal diffusivity of the path to the sample. As soon as anywhere between temperature sensor and sample and/or within the sample a phase shift and a change in maximum amplitude develop during the modulation, it is impossible to handle the analysis with Eq. (2). The analysis becomes then much more complicated. Progress was made recently by studying TMDSC with sawtooth modulations [6, 36]. As long as the Fourier equation of heat flow holds, the solutions for different events in the DSC are additive. Steady state, however, is lost each time a sharp change of $\dot{T}_s$ occurs. An empirical solution to this problem was to modify Eq. (2), as is indicated in Eq. (3) [24]:

$$(C_s - C_r) = \frac{A_\Phi}{A_q}\sqrt{1+(\tau\omega)^2} \tag{3}$$

where τ is determined by measurements at different frequencies.

The value of τ does not only depend on the heat capacity of the reference calorimeter and the Newton's-law constant, as one would expect from Eq. (2), but also on the mass and thermal conductivity of the sample and on all involved thermal contact resistances. Furthermore, the nature of τ depends also on the calorimeter type, and naturally also on any possible cross-flow between the sample and reference calorimeters. The empirical Eq. (3) can be assessed by a plot of the inverse of the uncorrected heat capacity in Eq. (3) *vs*. the square of the frequency. Only with periods longer than 250 s did the square root term in Eq. (3) become negligible for the analysis of heat capacities in typical commercial calorimeters. For shorter periods, reaching down to about 5 s, τ remained however a continuous function of the frequency ω, approaching at longer periods a value that is independent of ω. Naturally, to conduct a series of measurements at many frequencies at every temperature is a considerable increase in effort to establish the heat capacity. This difficulty led to a more extensive effort to make the required measurements at different frequencies in a single run [36]. In this paper, it will be shown how similar data on heat capacity, as well as the reversing and non-reversing components of an apparent heat capacity, can be established using the simple analysis method of the standard DSC of Eq. (1).

Analysis of a sawtooth modulation using standard DSC methods

During each segment of heating or cooling in a sawtooth modulated run, the thermal response will need 30 s or more to approach steady state. For an analysis with the standard DSC method, the initial data after each change in the rate of change of temperature must be discarded until steady state is reached [37]. After the baseline subtraction, only the data close to the upper and lower limits of $\Phi(t)$, just before the heating rate will be switched, give the steady state data to be inserted into Eq. (1). If the heating or cooling segments are too short to attain steady state and minimal temperature gradients within the sample, Eq. (1) does not give useable results. A careful in-

spection of the heat-flow rate can usually identify the point where the standard DSC analysis becomes possible. Furthermore, it may be possible during transitions to extrapolate the sample temperatures and heat-flow rates to steady state or to modify the modulation mode to find the steady state experimentally.

The constant rate of temperature change on heating or cooling for Eq. (1), q_h or q_c, is given by the slope of the sample temperature along the points which are in steady state. According to Eq. (1), the reversing specific heat capacity, $mc_{p,rev}$, is then given by:

$$mc_{p,rev} = \frac{\Phi_h - \Phi_c}{q_h - q_c} \tag{4}$$

Note that under the linearity condition of thermal response, Φ is positive (endothermic) on heating and negative (exothermic) on cooling. Analogously, the rates of temperature change q_h and q_c change their sign on going from heating to cooling.

In current TMDSC the non-reversible contribution of the latent heat can only be assessed indirectly by subtracting the reversing heat capacity from the total heat capacity or by an analysis in the time domain. Any error in the reversing as well as total heat capacity will then be transferred to the non-reversing heat capacity. The analysis using standard DSC methods allows a direct measurement of the non-reversing heat capacity by determining the difference in the heat capacities at their steady state. We call this quantity the imbalance in heat capacity and write, using Eq. (1):

$$mc_{p,imbalance} = \frac{\Phi_h}{q_h} - \frac{\Phi_c}{q_c} \tag{5}$$

The advantage of the imbalance in heat capacity over the non-reversing heat capacity is that it is a directly measurable quantity of the non-reversible contribution and avoids, as long as the conditions of standard DSC are fulfilled, the potential errors of the non-reversing heat capacity.

The irreversible heat-flow rate can be calculated from Eq. (5) by separating Φ_h and Φ_c into its reversible, underlying, and irreversible contributions ($\Phi_{h,rev}$, $\Phi_{h,und}$, and $\Phi_{h,irrev}$, and the respective cooling heat-flow rates):

$$mc_{p,imbalance} = \frac{\Phi_{h,rev} + \Phi_{h,und} + \Phi_{h,irrev}}{q_h} - \frac{\Phi_{c,rev} + \Phi_{c,und} + \Phi_{c,irrev}}{q_c} \tag{6}$$

Assuming linear response among the heat-flow rates caused by the true heat capacity, the following equality holds:

$$\frac{\Phi_{h,rev} + \Phi_{h,und}}{q_h} = \frac{\Phi_{c,rev} + \Phi_{c,und}}{q_c} \tag{7}$$

and:

$$mc_{p,imbalance} = \frac{\Phi_{h,irrev}}{q_h} - \frac{\Phi_{c,irrev}}{q_c} \tag{8}$$

Under conditions of stationarity $\Phi_{h,irrev}=\Phi_{c,irrev}=\Phi_{irrev}$, so that one can write:

$$\Phi_{irrev} = \frac{mc_{p,imbalance}}{\frac{1}{q_h} - \frac{1}{q_c}} \tag{9}$$

Data-treatment examples

The analysis of the sawtooth modulation with the standard DSC methods, described in the previous section, makes use of Eqs (1) and (4) for $c_{p,total}$ and $c_{p,rev}$, respectively, and the imbalance is the third measured quantity [$c_{p,imbalance}$ of Eq. (5)]. Figure 1a illustrates the deconvolution of the sample temperature by standard DSC analysis for a sawtooth of heating rates of 4.0 K min^{-1} (1/15 K s^{-1}), alternating with cooling rates of 2.0 K min^{-1} (1/30 K s^{-1}). A modulation period of 60 s yields then an underlying heating rate of 1.0 K min^{-1}. The first cycle of the sawtooth starts at T_0, the next at T_1, etc. The reversing pseudo-isothermal modulation has an amplitude of 1.5 K with the rates of temperature-change alternating between q_h=3.0 and q_c=–3.0 K min^{-1}, as indicated in the figure.

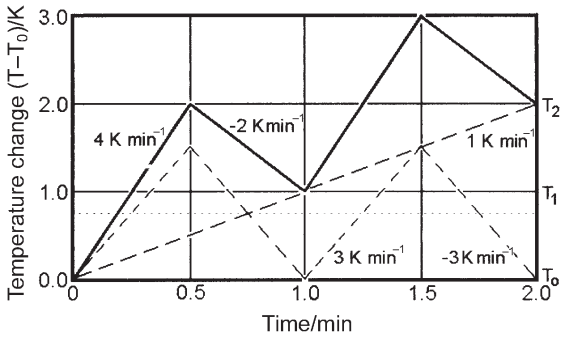

Fig. 1a Schematic drawing of sawtooth-type modulation (solid line) and its deconvoluted underlying heating rate $\langle \dot{T} \rangle$ and reversing rate of temperature change of ±3 K min^{-1} (dashed lines). The temperatures listed on the right indicate the beginnings and ends of the cycles

Assuming an instantaneous, linear response, the changes in the heat-flow rate are seen in Fig. 1b. The measured response $\Phi(t)$ is represented by the heavy line which has a meander-like shape, jumping from zero to the heating response in heat-flow rate, Φ_h, to the cooling response Φ_c, and vice versa. If the responses were not instantaneous, one would have had to wait until the steady states are reached and then extrapolate the steady state response back to the beginnings of the heating and cooling segments. This extrapolation produces a result similar to the one shown in Fig. 1b. For a heat capacity that changes linearly with temperature, the same analysis would still be possible, but a sudden or non-linear change during the modulation may destroy the stationarity [5, 38, 39].

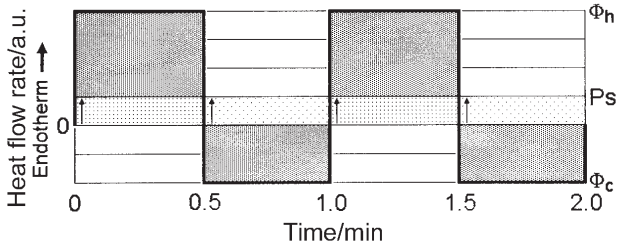

Fig. 1b Schematic drawing of the linear thermal response (solid lines) for the temperature program of Fig. 1a. The effects of the underlying (lightly dotted boxes) and reversing responses (heavily dotted boxes) are indicated. The heavy line represents $\Phi(t)$, and the pseudo-isothermal level (PS), the zero level and the value of Φ_h and Φ_c are marked

Assuming the heat capacity of the sample in Fig. 1a is C (in J K^{-1}), the value of the heat-flow rates can be calculated from Eq. (1) to be $\Phi_h=Cq_h=C/15$ W and $\Phi_c=Cq_c=-C/30$ W (note that for these calculations the values of q are in K s^{-1}). The total heat flow, ΔQ, is the integral (sum) of the heat-flow rates over one period of time, $\Delta Q=30C/15+30(-C/30)=C$ J. The value of ΔQ is also equal to the integral of C over the change in temperature, $\Delta Q=C(T_1-T_0)=C$ J, as expected in the absence of latent heats. The total heat-flow rate, $<\Phi(t)>$, is then equal to $\Delta Q/60$.

The reversible heat-flow rate is deconvoluted by subtracting $<\Phi(t)>$ from $\Phi(t)$. During the heating segment $<\Phi(t)>$, the lightly and vertically dotted area, is part of the positive heat-flow rate Φ_h. During the cooling segment, $<\Phi(t)>$ marked as the lightly and diagonally dotted area, is opposite in direction of the negative heat-flow rate and must be added to Φ_c and defines the pseudo-isothermal baseline level (*Ps*). In this case the position of *Ps* is raised above zero, as indicated in Fig. 1b. Above and below *Ps* the reversible heat-flow rate can be visualized as $\Phi_{rev}=\pm C/20$ W ($q_{rev}=\pm 3/60$ s, Fig. 1a). The reversible heat capacity can be calculated from Eqs (1) or (4). Both give, as expected, the same result: $C_{p,rev}=C$ J K^{-1}. Equation (2) leads, naturally, also to the same value $A_\Phi=C/20$ W and $A_q=1/20$ K s^{-1}. The amplitudes are taken as half the difference between the upper and lower limits of the heating and cooling segments. Under the conditions of linear response, these two sawtooth amplitudes must be multiplied with the same factor to yield the amplitudes of their first harmonic of the Fourier series [6]. Finally, the imbalance and the irreversible heat-flow rate are zero for this reversible system, as seen from Eqs (5) and (9). Table 1 gives a summary of the results.

Next, one can add a constant, irreversible thermal process with a latent heat, as is found for instance on cold crystallization of poly(ethylene terephthalate) or the curing of a thermoset [33]. A latent heat does not change the temperature changes of Fig. 1a, but the heat-flow rates need to be modified, as is shown in Fig. 1c. The heat-flow rate due to the exotherm was given the constant value of $-C/60$ W and compensates then the heat-flow rate of the underlying heating rate. Linearity of the thermal response with the temperature change has now been lost, but the stationarity still exists. The additional heat-flow rates are indicated by the two types of vertically shaded boxes. The observed heat-flow rates are marked by the heavy-line meander

and marked Φ_h and Φ_c, as before. The heat-flow rates, due to the underlying heating rate and the exothermic reaction cancel each other, leading to values of zero for the total heat flow, ΔQ, and total heat flow rate, $<\Phi(t)>$. The reversible heat flow rate about *Ps*, which has moved to the zero level because of the latent heat, is the same as in Fig. 1b. Equation (5) gives a heat capacity imbalance of $-3C/4$ J K^{-1}, and Φ_{irrev}, according to Eq. (9), is equal to $-C/60$ W, as was chosen as the value for the latent heat effect.

Table 1 Parameters derived from Figs 1b to 1e

Example	Φ_h[a]	Φ_c[a]	ΔQ[b]	$<\Phi(t)>$[c]	Φ_{rev}[d]	$C_{p,rev}$[e]	$C_{p,imbalance}$[f]	Φ_{irrev}[g]
	W		J	W			J K^{-1}	W
Fig. 1b	$C/15$	$-C/30$	C	$C/60$	$\pm C/20$	C	0	0
Fig. 1c	$C/20$	$-C/20$	0	0	$\pm C/20$	C	$-3C/4$	$-C/60$
Fig. 1d	$C/12$	$-C/60$	$2C$	$C/30$	$\pm C/20$	C	$+3C/4$	$+C/60$
Fig. 1e	$C/12$	$-C/30$	$1.5C$	$C/40$	$\pm 7C/120$	$7C/6$	$+C/4$	$(+C/180)$[h]

[a]Calculated from Eq. (1)
[b]Integration of $\Phi(t)$ over one modulation cycle with respect to t
[c]From pseudo-isothermal analysis by averaging $\Phi(t)$ over one modulation cycle
[d]By subtraction of $<\Phi(t)>$ from $\Phi(t)$
[e]From Eqs (2) or (4)
[f]From Eq. (5)
[g]From Eq. (9). The non-reversing heat-flow rates give identical values and can be calculated using $\Phi_{nonrev}=<\Phi(t)>-C_{p,rev}<q>$
[h]Value from Eq. (9) which does not apply because non-stationarity

The meaning of the imbalance in heat capacity can be gathered from this example. During the heating segment with 4 K min^{-1}, for 0.5 min, the measured heat capacity is not the true heat capacity of C J K^{-1}, but an apparent heat capacity, increased by the exotherm to $3C/4$ J K^{-1}. Analogously, the apparent heat capacity on cooling at 2 K min^{-1} is $3C/2$ J K^{-1}, increased by the exotherm, but by more than on heating because of the smaller temperature decrease on cooling. The imbalance of the two apparent heat capacities is $-3C/4$ J K^{-1} as given by Eq. (5). Equation (5) represents the difference between the apparent heat capacities on heating and cooling, as changed by the constant, irreversible latent heat, and Eq. (9) gives the constant, irreversible heat-flow rate, as set.

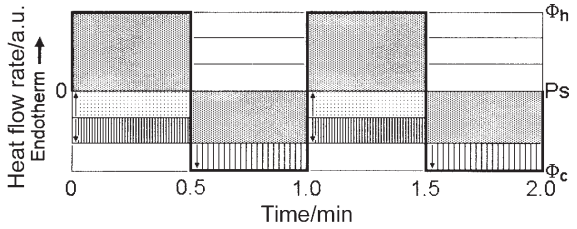

Fig. 1c Schematic drawing of the thermal response as in Fig. 1b, but with the addition of an irreversible, exothermic latent heat represented by the vertically shaded areas (non-linear but stationary)

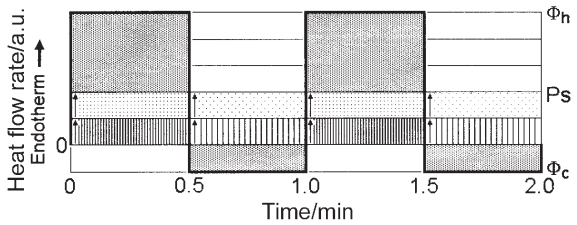

Fig. 1d Schematic drawing of the thermal response as in Fig. 1b, but with the addition of an irreversible, endothermic latent heat represented by the vertically shaded areas (non-linear but stationary)

The case with an endothermic, constant, irreversible latent heat is illustrated in Fig. 1d. Such endotherm may occur in the presence of slow pyrolysis, sublimation, or melting which are not affected by the modulation. The normal melting of macromolecules also shows endotherms, but the heat of fusion absorbed is usually not constant on modulation of temperature [18]. Crystallization, shown in the example of Fig. 1b, occurs on cold crystallization with so much supercooling that the changes in temperature due to modulation do not change the rate of crystallization significantly. The equivalent melting rates of crystals without effect of modulation due to superheating do not exist. On melting, superheating is usually small, so that substantial changes of melting-rate occur on modulation [18]. The heat-flow rate due to the endotherm was assumed to be fixed to $+C/60$ W, at the same value as the heat-flow rate due to the underlying heating rate. The heat-flow rate due to the endotherm is indicated by the vertically shaded boxes. The observed heat-flow rates on heating and cooling, Φ_h and Φ_c, are changed as marked in Fig. 1d. The level of *Ps* about which the pseudo-isothermal oscillation occurs, is raised even further than in Fig. 1b. The total heat-flow rate due to the underlying heating rate and the endothermic reaction is indicated by the difference between *Ps* and zero as $C/30$ W, leading to a total heat flow of 2.0 *C* J per cycle. The reversible heat-flow rate about *Ps* is the same as in Figs 1b and 1c. With $\Phi_h=5C/60$ W and $\Phi_c=-C/60$ W, Eq. (5) gives a heat capacity imbalance of $3/4C$ J K^{-1} and Φ_{irrev} is equal to $+C/60$ W according to Eq. (9), as was assumed in the design of the example.

If an irreversible process changes abruptly within the modulation cycle, an error occurs in the estimation of the reversing heat capacity due to a loss in stationarity [5]. Furthermore, the time to the approach to steady state may be lengthened due to the irreversible process and exceed the time of modulation. In reality, thus, a heat-flow rate curve with an irreversible process may look much more complicated than shown in Figs 1c and d, and then needs to be studied in more detail. Using the standard DSC method, however, this study is much simpler than sorting the various contributions to the higher harmonics in distorted apparent heat capacities in TMDSC.

Figure 1e illustrates the case of an irreversible latent heat endotherm of a heat-flow rate of $C/60$ W on heating only (compare to Figs 1d and 1b). This corresponds to a melting process that does not continue and is not followed by recrystallization on cooling, as is common in polymers. Such combination is non-linear

and non-stationary since it changes abruptly within the modulation cycle. The latent heat contributions marked by the vertically shaded boxes increasing Φ_h to $5C/60$ W and Φ_c remains at $-2C/60$ W, so that ΔQ is equal to $1.5C$ J and the total heat-flow rate is $C/40$ W. The pseudo-isothermal level is raised to 1.5 $C/60$ W, as shown, so that Φ_{rev} is $\pm 3.5C/60$ W. Equation (4) results in an apparent reversible heat capacity of $7C/6$ J K^{-1}, and the imbalance in heat capacities is $+1/4C$ J K^{-1} according to Eq. (5). During the heating segment with 4 K min^{-1} for 0.5 min, the measurement does not give the true heat capacity C J K^{-1}, but an apparent heat capacity of $1.25C$ J K^{-1}. The heat capacity on cooling at 2 K min^{-1} is, as assumed, C J K^{-1} and accounts for the remaining imbalance. The irreversible heat-flow rate cannot be calculated from Eq. (9) because of the loss of stationarity. From the assumption made for the drawing of Figs 1d and 1b and Eq. (6), it is obvious that $\Phi_{h,irrev} = C/60$ W and $\Phi_{c,irrev}$ is zero, and Φ_{irrev} cannot be the $C/180$ W shown in parentheses in Table 1.

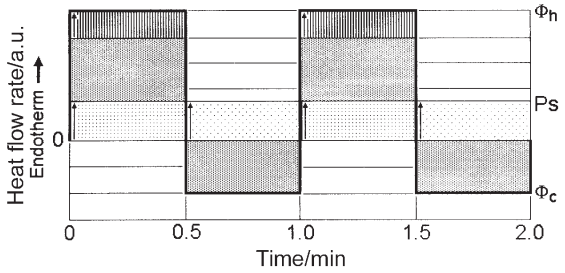

Fig. 1e Schematic drawing of the thermal response as in Fig. 1b, but with the addition of an irreversible, endothermic latent heat during the first half of each cycle as represented by the vertically shaded areas (non-linear and non-stationary)

In comparison to the analysis based on standard DSC, the TMDSC analysis leads with Eq. (2) to the correct reversing heat capacity of $7C/6$ J K^{-1}, as also shown in Table 1. With the total heat capacity as calculated from Eq. (1) of $1.5C$ J K^{-1}, this yields because of the non-stationarity to an erroneous non-revering heat capacity ($C/3$ J K^{-1}) and the same wrong non-reversing heat-flow rate as shown in Table 1 ($+C/180$ W). The imbalance of heat capacity calculated with Eq. (5), in contrast, is a correct quantity and the source of error for the incorrect irreversible heat-flow rate can be traced easily, as shown above.

Experimental details

The heat capacity measurements were performed with a Perkin-Elmer Pyris-1 TMDSC with a CryoFill™ liquid nitrogen cooler. The calorimeter was calibrated with the melting points of ice (273.15 K), indium (429.75 K) and tin (505.03 K) for the sample temperature and with the heat of fusion of indium (28.45 J g^{-1}) for the preliminary value of Φ during 10 K min^{-1} scanning. The purge gas was pure helium, flowing with a rate of 25 mL min^{-1}.

Granular poly(ethylene terephthalate) (PET) from Scientific Polymer Product Inc. (#57) was used as the only sample and weighed with a Cahn-28 electrobalance. Before measurement the samples were treated as follows: The granular sample (about 20 mg) was lightly pressed at 563 K to get a good contact with the pan bottom, followed by quenching on a surface of ice, then crimped.

Three parallel runs were performed for an empty pan, the sample pan, and the reference material pan to be able to use Eq. (4) with the calibrations described above. The reference material was sapphire (26.026 mg) in a flat piece, supplied by the Perkin-Elmer Instruments Co. The data of the heat capacity of sapphire for the point-to-point calibration were taken from the critical survey available in the literature [35].

The program of temperature modulation consisted of heating at 4.0 K min^{-1} for 2.0 K followed by cooling at 2.0 K min^{-1} for 1.0 K, so that the period is 60 s, as illustrated in Fig. 1a. Within each cycle, the upper and lower limits of the heat-flow rate Φ_h and Φ_c, respectively, are read from the baseline-subtracted curve. The corresponding rate of temperature change q_h is read from the slope of the sample temperature between 0.3 and 0.5 min into the modulation cycle, while the corresponding q_c is read from the slope of the sample temperature between 0.8 and 1.0 min. The reversing heat capacity is then calculated from Eq. (4), and the imbalance in heat capacity from Eq. (5). The total heat flow ΔQ is the integral of the heat-flow rate over this cycle, and the total heat capacity is the total heat-flow rate divided by the underlying heating rate $<q>$ according to Eq. (1) ($<\Phi(t)>=\Delta Q/60$). The non-reversing heat capacity is the difference between the total heat capacity and the reversing heat capacity which is calculated from Eq. (4).

Both the helium purge gas and liquid nitrogen cooler facilitate the fast approach to a steady state, but do not favour long-term stability of the thermal response between different runs, especially when the heating rate is slow [40]. The baseline subtraction, therefore, needed further correction with intermittent isotherms. In the transition regions, longer baseline extrapolations were necessary since the sample would undergo changes during isotherms.

The cold crystallization and the annealing of crystallites in the melting range of PET were also analyzed by quasi-isothermal modulation ($<q>=0$). The rate of temperature change was in this case ± 2.0 K min^{-1}. The modulation period of 1.0 min gave an amplitude of 1.0 K.

Results

The total heat capacity of the TMDSC run for PET is shown in Fig. 2. It covers the glass transition, cold crystallization, and a wide melting range and was generated with the temperature modulation depicted in Fig. 1a. Despite the rather large shift of the baseline and long-term instability which led to a lesser precision of the total heat capacity, a quantitatively acceptable, apparent reversing heat capacity could be extracted due to the new evaluations once every kelvin of temperature change. The results are shown in Fig. 3, together with calculations of the imbalance and non-reversing heat capacities, based on the above described analysis of the sawtooth

modulation. For comparison, the Athas Data Bank information for amorphous PET is also plotted as the points •.

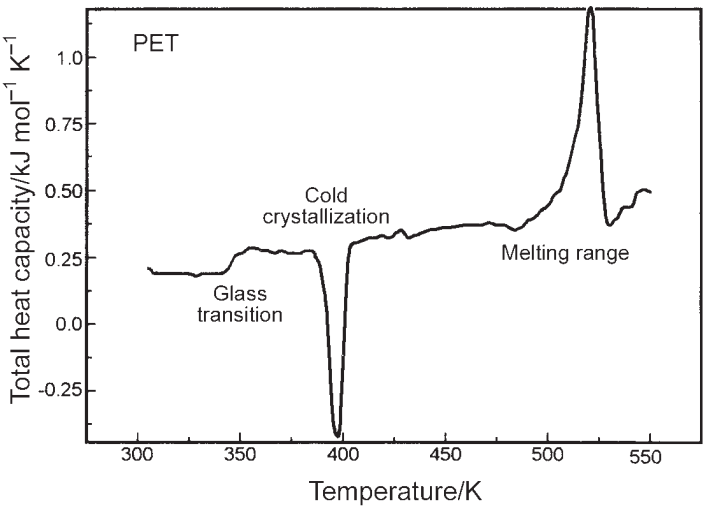

Fig. 2 Total heat capacity of PET deconvoluted from a run as given in Fig. 1a from 315 to 555 K (240 sawtooth modulation cycles)

The cold crystallization in the temperature range (380–420 K) was analyzed in more detail by running quasi-isothermal experiments with a sawtooth modulation of rates of temperature change of ±2 K min^{-1} and periods of 1.0 min. The results are shown in Fig. 4. The reversing heat capacity (+) decreases on cold crystallization as expected from the lower heat capacity of the crystalline sample, but shows no latent heat contribution as could be seen already from Fig. 3. The same decrease in true heat capacity can be calculated from the integral of the total heat-flow rate over time in terms of the latent heat evolved which was then converted to crystallinity, and used for the estimation of the heat capacity as sum of contribution of amorphous and crystalline fractions to the heat capacity and is indicated in Fig. 4 as (•). Both amorphous and crystalline heat capacities are known from the Athas Data Bank. The imbalance in heat capacity (▲) is calculated from Eq. (5) and illustrates the kinetics of the cold crystallization.

Figure 5 illustrates a similar quasi-isothermal analysis in the melting range at 520 K. The decrease of the reversing heat capacity, as calculated with Eq. (4), and the imbalance in heat capacity, as evaluated by Eq. (5), is plotted as a function of time indicated by the symbols (+) and (▲), respectively. The chosen temperature is close to the peak of melting with an underlying heating rate of 1.0 K min^{-1} as shown in Fig. 3. Both, the reversing heat capacity and the imbalance decrease with time. These results on PET should be compared with the much more extensive work carried out with sinusoidal modulation and analysis by Fourier analysis [41–43].

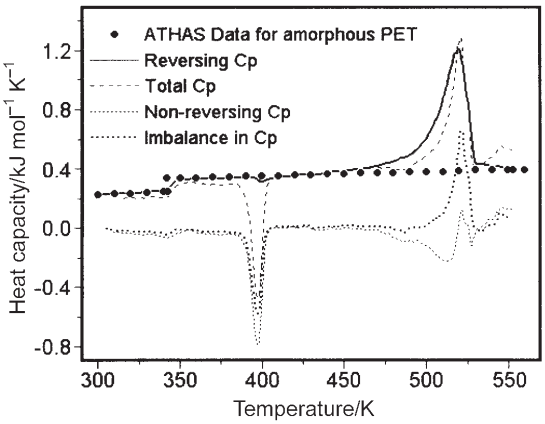

Fig. 3 Analysis of the data from Fig. 2 with the standard DSC method. Reversing heat capacity from Eq. (4), total heat capacity from Eq. (1) with the total heat-flow rate and underlying heating rate, non-reversing heat capacity from the difference between reversing and total heat capacity, and imbalance of heat capacity from Eq. (5). Also listed are the data bank data for the heat capacity of amorphous PET

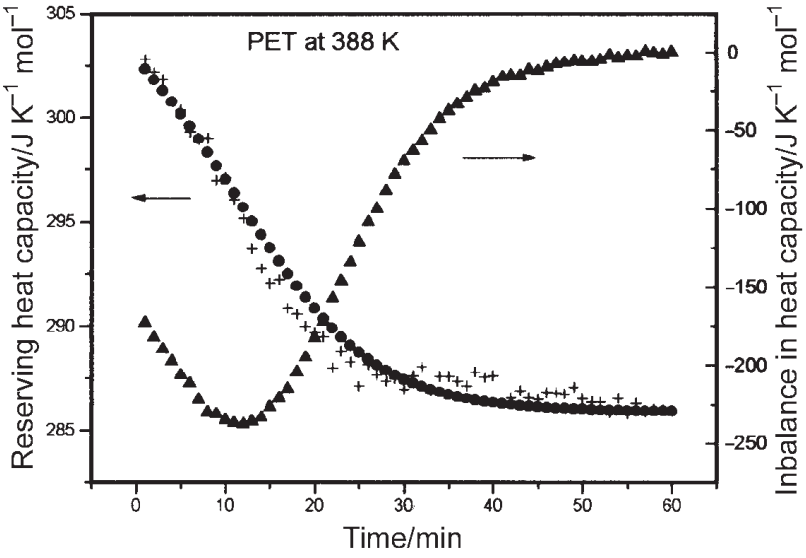

Fig. 4 Reversing heat capacities and the imbalance in heat capacities (triangles) of PET during cold crystallization at 388 K in a quasi-isothermal measurement with a sawtooth modulation with rates of temperature change of 2 K min^{-1} and a period of 1.0 min (amplitude 1.0 K). The data for the crosses are calculated from the upper and lower limits of the heat flow rates [Eq. (2)], and the data for the filled circles are calculated from the integral of the total heat-flow rate over the annealing time

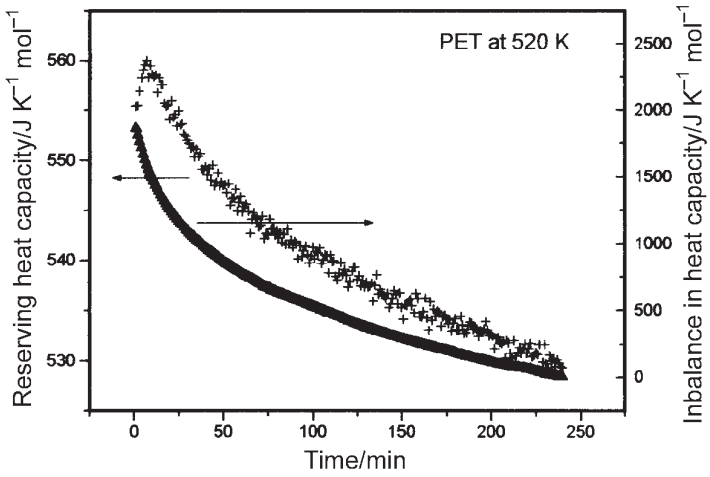

Fig. 5 Reversing heat capacities (crosses) and the imbalance in heat capacities (triangles) of PET during a quasi-isothermal measurement at 520 K, using the quasi-isothermal analysis under conditions as in Fig. 4

Discussion

The analysis method described with help of Fig. 1 permits the study of reversible and reversing processes in a similar and possibly even more detailed manner than the commonly carried out TMDSC based on the Fourier analysis of the temperature modulation and the sample response, as given by Eqs (2) and (3). As seen in the various forms of carrying out the standard DSC based on sawtooth, step-isotherm, or step-scan methods [23–31], a multitude of analyses of the obtained results are possible. As a typical example of the discussion of the modulation cycles of PET in the melting range, the baseline-subtracted data are displayed in Fig. 6 for the temperatures of 450.8 K (before major melting starts) and 512.2 K (within the major melting peak).

The low-temperature measurement is drawn in dashed lines. It is a standard analysis and can easily be related to Fig. 1b with results analogous to the ones listed in Table 1. The approaches to steady state from 0 to 0.3 and 0.5 to 0.8 min are replaced by extrapolation to a horizontal (or slightly sloping) steady-state heat-flow rate and used as values for Φ_h and Φ_c, as indicated. The zero level and level *Ps* had to be established from occasional zero baselines included in the sawtooth modulation, or derived from a baseline measurement. In the present attempt the baseline was insufficiently constant to display these details. A slight change in heat capacity with time is noticeable. A detailed comparison reveals that the change in heat capacity with temperature is slightly asymmetric, indicating some irreversible behavior. This is expected, since the level of heat capacity is above that given by the data bank [32] for the level of crystallinity and small reversible and non-reversible effects have been identified in this temperature region [41, 42]. Even at this lower level of precision, it is thus possible to undertake further data refinement.

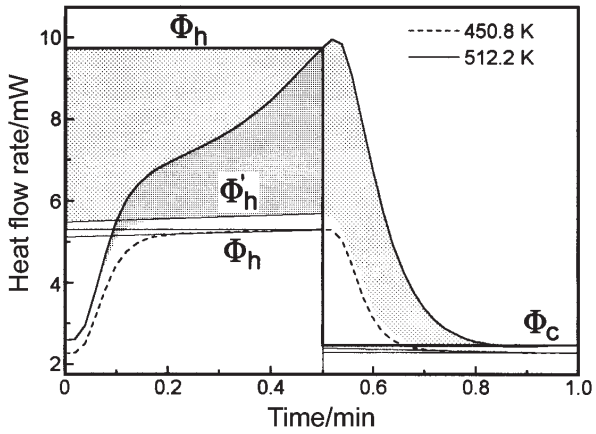

Fig. 6 Baseline-subtracted heat-flow rates of PET for a single sawtooth at 450 and 512 K from the experiment of Fig. 2

Much more obvious deviations from a reversible behavior are seen in the data taken at 512.2 K. The first observation is that on heating, a large latent heat is absorbed and steady state is not reached. On cooling, however, steady state is approached with only a very small indication of an exotherm at about 0.9 min into the modulation cycle. At 0.5 min into the modulation, the melting is interrupted by beginning of the cooling cycle, but further latent heat of fusion is contributed as seen up to 0.8 min. The analysis is now similar to the analysis of Fig. 1e, except that the melting contribution changes throughout the modulation cycle and is even further from stationary than in Fig. 1e. Comparing the heat-flow rate to the data taken at 450.8 K allows, however, an approximate separation of the melting, as marked by the vertical shading in the heating segment and the diagonal shading in the cooling segment of the modulation cycle. Comparing the diagonally shaded areas in the heating and cooling segments suggests a rough equivalence, so that the marked Φ_h accounts for practically all the irreversible melting in the heating segment. The cooling segment, however, when represented by Φ_c, contains no latent heat, and similarly, the heat-flow rate Φ'_h is a measure of the heat-flow rate on heating without latent heat. Further analysis is now possible using the basic analysis for Fig. 1e with results similar to the ones displayed in Table 1.

The limits of the analysis with non-stationary latent heat effects can also be seen. At 0.5 min into the modulation cycle, the melting up to the corresponding temperature is not complete, i.e., it will be added on continuing the analysis to the next cycle, distorting the overall observed melting peak. Once noticed, more experimental details can, naturally, be generated by designing and testing a sawtooth that avoids the melting peak distortion by insertion of an isothermal segment after the time of 0.5 min, for example. This method was applied in the detailed analysis of the melting of In as affected by instrument parameters [44, 45]. In such analyses it must naturally be considered that the polymer crystals are not fixed entities. They can anneal (with a

small exotherm), and for different heating protocols different results are expected, as was studied in detail when analyzing crystallization and melting of polyethylene copolymers by DSC and TMDSC [20, 21]. For the study of reversible melting, all irreversible melting must be removed as is attempted with the assignment of Φ'_h, but quasi-isothermal experiments without an underlying heating rate are more suitable for such analysis, as will be shown below.

To analyze reversible specific heat capacities without latent heat effects one can turn to Fig. 3 and study the temperature regions below the glass transition and after melting. The data are in agreement with the data bank within the precision of the standard DSC method. The analysis is carried out as discussed in connection with Figs 1a and 1b. This calculation is not affected by the long-term shift of asymmetry between the different runs since each separate cycle is analyzed independently over a sufficiently small temperature range so that the change in asymmetry is minor and can be neglected, providing one of the basic advantages of temperature modulation.

Due to the neglect of the data during the approach to steady state, and uncertainties of temperature gradients within the sample, the analysis by standard DSC is not as precise as possible by the full Fourier analysis [23–26]. But, one can see from Fig. 3, as in sinusoidally-modulated TMDSC [1–3], that the glass transition is almost reversible and occurs prominently in the total and reversing signals [8–16], while cold crystallization is almost irreversible and occurs only in the total and non-reversing signals [1–3].

The cold crystallization in the temperature range of 380–420 K is a nucleated, irreversible process [18, 33] with an exothermic latent heat without reversal on cooling, as described in with Fig. 1c, above. Stationarity of the thermal response is approximated for each cycle. As observed in Fig. 3, the reversing heat capacity remains at the vibrational heat capacity. More details of the heat capacity and enthalpy of crystallization are given below by analyzing the quasi-isothermal experiment of Fig. 4. The imbalance in heat capacity of Eq. (5) is sensitive to a small enthalpy relaxation at the glass transition, the irreversible exotherm of cold crystallization, a small exotherm at about 475 K, and the melting endotherm, with some differences from the non-reversing signal of TMDSC. The main difference occurs at the melting endotherm, where the exotherm disappears.

In the melting range, a gradual increase in total and reversing apparent heat capacity is followed by the main melting peak. This apparent heat capacity is not indicated mainly as irreversible, as expected, but has both contributions from the reversing and imbalance as given by Eqs (4) and (5). Clearly these are artifacts when analyzed without an effort to separate the latent heat effects properly as indicated in the discussion of Fig. 6. The heat capacity imbalance starts to indicate a shallow exotherm at about 425 K suggestive of annealing of the crystals during heating, as can also be seen on TMDSC with modulation 'without cooling', a method that matches underlying heating rate and modulation so that the lowest rate of temperature change is zero [46]. The same exotherm appears in the non-reversing signal of Fig. 3. While the non-reversing heat capacity in the peak region between 500 and 525 K reveals only the difference between the total and reversing signals, the imbalance heat

capacity shows clearly the positive effect of the melting in the heating as well as in the cooling segments of the modulation cycle, as derived from Figs 1e and 1d, respectively, and listed in Table 1. The discussion of Fig. 6, above, illustrates how information can be extracted even in this region of extreme non-stationarity. The imbalance in heat capacity as a directly measured quantity may be more advantageous in the analysis than the non-reversing heat capacity which is an indirect quantity.

Quasi-isothermal TMDSC measurements can trace the evolution of the phase transitions by following the reversing heat capacity in case of slow processes. Figure 4 illustrates the continuous decrease in reversing heat capacity calculated from Eq. (4) during cold crystallization at 388 K. Since it agrees well with the increase in crystallinity calculated from the integral of the total heat-flow rate as derived in the example of Fig. 1c for an underlying heating rate of zero, it is clear that the measured reversing heat capacity is truly reversible and measures the kinetics of transformation of the amorphous polymer to crystals. If we assume that the exotherm does not change much during each individual one-minute modulations, the imbalance in heat capacity calculated from Eq. (5) is initially a measure of the self-acceleration of the crystallization. As the nucleated crystals form with a constant linear growth rate, the surface area increases and with it the volume of crystals builds faster than the linear dimensions and $c_{p,imbalance}$ becomes more negative. As the crystals impinge or are hindered in further growth by restrictions from the amorphous phase, the growth rate decreases and finally approaches zero, as shown in Fig. 4. Such decrease in crystallization rate due to impingement is often described by the Avrami equation [18]. The link to quantitative data can be made using Eqs (5) and (9) and typical data can be seen in Table 1 for the example of Fig. 1c.

Quasi-isothermal TMDSC measurements can also extract information on an underlying truly reversible transition by extrapolating the data of a slowly decaying reversing processes to infinite time. In the case of melting of polymers a truly reversible melting could be proven. Some of such reversible crystallization processes on quasi-isothermal TMDSC curve have been discussed and may be linked to models of polymer structure [20, 21, 42, 46]. The same effect can be seen in Fig. 5 for a quasi-isothermal analysis at 520 K. The parallel, slow decrease of the imbalance in heat capacity towards zero at a heat capacity still larger than expected for the remaining crystallinity indicates the presence of a small amount of reversible latent heat that must be added to the true heat capacity. The irreversible annealing exists over quite a long time and negates any quantitative interpretation of an analysis with an underlying heating rate. The sample changes continuously during analysis. Overall, the imbalance of heat capacity is positive, a sign that the endothermic effect is overwhelming and ultimately disappears (Figs 1d and 1e and Table 1). The interpretation of this fact is that on each modulation cycle some more melting occurs than recrystallization (compare data of Fig. 1d and 1c in Table 1). Initially, at less than 10 min in Fig. 5, the imbalance is less and was shown to be connected to some exothermic process [41]. The explanation of these observations is simple. An exothermic process can account for either recrystallization or annealing to more stable crystals which melt sufficiently higher not to be melted again in the next quasi-isothermal cycle. An endother-

mic excess, in contrast, shows that some molecules that underwent partial melting before where now melted completely and can then not recrystallize because of a lack of molecular nucleation. After a sufficient number of cycles have occurred, a steady state has been reached at the crystal surfaces with truly reversible partial melting of molecules without the need of molecular nucleation [18]. More details about reversible endotherms in the melting range of polyethylene are given in [20, 21, 46].

Conclusions

Data of the sawtooth-type, temperature-modulated DSC can be produced and analyzed with the standard DSC method as expressed in Eqs (1), (4) and (5). The calculations are carried out without Fourier transformation as needed for typical TMDSC and are simpler, and often even more transparent (Fig. 6). The overall calorimetric precision is limited to that of the standard DSC, but the times for measurement and data analysis may be significantly less. The linearity and stationarity conditions of the thermal response can be demonstrated to be a prerequisite of the validity of reversing heat capacity as well as of the non-reversing heat capacity in the same way as they are in TMDSC with Fourier analysis (Fig. 1 and Table 1). A third, directly measurable quantity, the imbalance in heat capacity, is defined with Eq. (5). As an example, PET is analyzed by the method of temperature modulation with the standard DSC. Most of the large reversing and non-reversing heat capacities in the melting range are shown to be artifacts due to non-linearity seen in Figs 3 and 5 coupled with the non-stationarity illustrated in Fig. 6. Quasi-isothermal measurements, however, can be applied to the study of the decay of the irreversible processes and reveal the reversible melting as illustrated in Fig. 5. If stationarity is approximately preserved, as in the cold-crystallization region of Fig. 3, quantitative deconvolution is possible and the kinetics of the transition can be followed by either the change in reversible heat capacity or the change in imbalance in heat capacity [Fig. 4, and Eqs (4) and (5)]. The heat capacity in transition-free regions can be analyzed. In this case linearity and stationarity hold (<330 K and >530 K in Fig. 3). In the 'irreversible' glass-transition region, linearity and stationarity are sufficiently preserved at a fixed frequency, to permit a separation of enthalpy relaxation and perhaps even permit a study of the change of the glass transition with frequency. More detailed studies are necessary to reveal in this case the irreversible nature of the glass transition as was shown earlier [8–17]. The sawtooth modulation may be particularly suited for this analysis, since it can be deconvoluted into the sample response to several simultaneously acting frequencies of temperature change [47]. For such analysis, however the various Fourier components must be isolated [6, 24, 36] complicating the here presented simple analysis method.

* * *

This work was supported by the Division of Materials Research, National Science Foundation, Polymers Program, Grant #DMR-9703692 and the Division of Materials Sciences and Engineering, Office of Basic Energy Sciences, U.S. Department of Energy at Oak Ridge National Laboratory, man-

aged and operated by UT-Batelle, LLC, for the U S. Department of Energy, under contract number DOE-AC05-00OR22725.

References

1 M. Reading, Trends in Polymer Sci., 8 (1993) 248.
2 M. Reading, D. Elliot and V. L. Hill, J. Thermal Anal., 40 (1993) 949.
3 P. H. Gill, S. R. Sauerbrunn and M. Reading, J. Thermal Anal., 40 (1993) 931.
4 B. Wunderlich, Y. Jin and A. Boller, Thermochim. Acta, 238 (1994) 277.
5 M. Merzlyakov and C. Schick, Thermochim. Acta, 330 (1999) 55.
6 B. Wunderlich, A. Boller, I. Okazaki, K. Ishikiriyama, W. Chen, M. Pyda, J. Pak, I. Moon and R. Androsch, Thermochim. Acta, 330 (1999) 21.
7 S. X. Xu, Y. Li and Y. P. Feng, Thermochim. Acta, 343 (2000) 81.
8 J. M. Hutchinson and S. Montserrat, J. Thermal Anal., 47 (1996) 103.
9 B. Wunderlich, A. Boller, I. Okazaki and S. Kreitmeier, J. Thermal Anal., 47 (1996) 1013.
10 J. M. Hutchinson and S. Montserrat, Thermochim. Acta, 286 (1996) 263.
11 B. Wunderlich and I. Okazaki, J. Thermal Anal., 49 (1997) 57.
12 S. L. Simon and G. B. McKenna, Thermochim. Acta, 348 (2000) 77.
13 A. Boller, C. Schick and B. Wunderlich, Thermochim. Acta, 266 (1995) 97.
14 A. Boller, I. Okazaki and B. Wunderlich, Thermochim. Acta, 284 (1996) 1.
15 L. C. Thomas, A. Boller; I. Okazaki and B. Wunderlich, Thermochim. Acta, 291 (1997) 85.
16 I. Okazaki and B. Wunderlich, J. Polymer Sci., Part B: Polymer Phys., 34 (1996) 1941.
17 B. Wunderlich, D. M. Bodily and M. H. Kaplan, J. Appl. Phys., 35 (1964) 95.
18 B. Wunderlich, Macromolecular Physics, Vol. 2, Crystal Nucleation, Growth, Annealing, Vol. 3, Crystal Melting, Academic Press, New York 1976, 1980.
19 A. Toda, T. Oda, M. Hikosaka and Y. Saruyama, Polymer, 38 (1997) 231.
20 R. Androsch and B. Wunderlich, Macromolecules, 32 (1999) 7238.
21 R. Androsch and B. Wunderlich, Macromolecules, 33 (2000) 9076.
22 B. Wunderlich, J. Phys. Chem., 69 (1965) 2078.
23 M. Pyda, Y. K. Kwon and B. Wunderlich, Thermochim. Acta, 367/368 (2001) 217.
24 R. Androsch, I. Moon, S. Kreitmeier and B. Wunderlich, Thermochim. Acta, 357/358 (2000) 267.
25 Y. K. Kwon, R. Androsch, M. Pyda and B. Wunderlich, Thermochim. Acta, 367/368 (2001) 203.
26 J. Pak and B. Wunderlich, Thermochim. Acta, 367/368 (2001) 229.
27 R. Riesen, G. Widmann and R. Truttmann, Thermochim. Acta, 272 (1996) 27.
28 B. Schenker, G. Widmann and R. Riesen, J. Thermal Anal., 49 (1997) 1097.
29 W. Sichina and R. Cassel, Proc. 28th NATAS Conf. in Orlando, FL, Oct. 4–6, K. J. Kociba and T. Kirchner-Jean, Eds, 28 (2000) 158.
30 B. Wunderlich, Thermochim. Acta, 5 (1973) 369.
31 Y. K. Kwon, A. Boller, M. Pyda and B. Wunderlich, Polymer, 41 (2000) 6237.
32 Advanced Thermal Analysis System, for a description see, for example B. Wunderlich, Pure and Applied Chem., 67 (1995) 1919. For values see the downloadable database on the internet, URL: http://web.utk.edu/~athas.

33 B. Wunderlich, Thermal Analysis, Academic Press, Boston, MA, 1990, or the updated computer course: Thermal Analysis of Materials, downloadable from the internet.
34 E. Gmelin and S. M. Sarge, Thermochim. Acta, 347 (2000) 9.
35 D. G. Archer, J. Phys. Chem. Ref. Data, 22 (1993) 1441.
36 B. Wunderlich, R. Androsch, M. Pyda and Y. K. Kwon, Thermochim. Acta, 348 (2000) 181.
37 B. Wunderlich, I. Okazaki, K. Ishikiriyama and A. Boller, Thermochim. Acta, 324 (1998) 77.
38 B. Wunderlich, J. Thermal Anal., 48 (1997) 207.
39 M. L. di Lorenzo and B. Wunderlich, J. Therm. Anal. Cal., 57 (1999) 459.
40 T. Hatakeyama and F. X. Quinn, Thermal Analysis, Fundamentals and Applications to Polymer Science, 2nd Ed., Wiley, Chichester 1999, p. 98.
41 I. Okazaki and B. Wunderlich, Macromolecules, 30 (1997) 1758.
42 I. Okazaki and B. Wunderlich, Macromol. Rapid Commun., 18 (1997) 313.
43 C. Schick, M. Merzlyakov and B. Wunderlich, Polym. Bull., 40 (1998) 297.
44 R. Androsch and B. Wunderlich, Thermochim. Acta, 364 (2000) 181.
45 R. Androsch and B. Wunderlich, Thermochim. Acta, 369 (2001) 67.
46 Proc. of the TA Instruments Modulated DSC Seminar and Training Course Oct. 25 and 26 (1999), as well as the Proc. 27th NATAS Conf. in Savannah, GA, planned for Sept. 19–22, K. R. Williams and K. Kociba, Eds 1999.
47 W. Hu, T. Albrecht and G. Strobl, Macromolecules, 32 (1999) 7548.
48 P. Kamasa, M. Merzlyakov, P. Pyda, J. Pak, C. Schick and B. Wunderlich, Thermochim. Acta, submitted, Proc. 28th NATAS Conf. in Orlando, FL, Oct. 4–6, K. J. Kociba and T. Kirchner-Jean, 28 (2000) 889.